31st Annual International Conference of the IEEE EMBS
Minneapolis, Minnesota, USA, September 2-6, 2009

Modeling Electrical Activities of a Growing Breast Cancerous Cell Based on a Semiconductor Approach

Ahmed Hassan, *Student Member*, *IEEE,* and Magda El-Shenawee, Senior *Member, IEEE*

***Abstract*—A two dimensional diffusion-drift model is developed to simulate the electrical activities of a breast cancerous cell during the hyperpolarization which occurs at the G1/S transition. The model focuses on calculating the temporal and the spatial patterns of the electric current densities and biopotentials generated at the cell boundary and its surroundings. Different durations for the hyperpolarization phase were studied. The results show that the electric signals generated in the tumor cell's surroundings increase as the duration of the hyperpolarization phase decreases or when the transition becomes faster.**

I. INTRODUCTION

THE biomagnetic (BM) and biopotential (BP) signals generated by growing breast tumors have recently received increasing attention for non-invasive and passive detection of breast cancer [1]-[3]. The BM and BP signals are naturally generated by growing tumors, and therefore, no harmful incident radiation is employed. In addition, the BM and BP detection techniques have the potential of characterizing breast tumors (as benign or malignant) without the need of biopsies [1]-[3].

In order to advance the BM and BP detection of breast cancer, however, the electric signals generated by growing breast tumors need to be modeled using mathematical biology methods. These models will help estimate the characteristics and features of the generated BM and BP signals and will provide in depth knowledge regarding the biophysics associated with tumor growth.

The mathematical model needs to calculate both the temporal and the spatial patterns of the tumor induced electric signals. The analysis is complicated by the fact that tumors generally exhibit irregular shapes [4]. This is unlike nerve fibers which can be approximated to some extent to have cylindrical symmetry [5].

This paper elaborates on some issues raised in [6] which proposes to use the diffusion-drift analysis to model the electrophysiological processes exhibited by dividing breast cancerous cells. The use of the diffusion-drift analysis is frequently employed in semiconductors, (see [7] for example) to model the transient electric current densities and potentials of multi-charged (electrons and holes) devices. The diffusion-drift analysis is adopted here for the BPs and electric current densities generated by a growing tumor cell.

Manuscript received April 2, 2009. This work is supported in part by the Doctoral Academy Fellowship (DAF) at the University of Arkansas and the National Science Foundation (NSF) award number ECS-0524042.

A. M. Hassan and M. El-Shenawee are with the Electrical Engineering Department, University of Arkansas, Fayetteville, AR 72701 USA (e-mail: amhassan@uark.edu and magda@uark.edu).

II. BIOPHYSICAL FOUNDATION FOR THE ELECTRIC SIGNALS INDUCED BY A MCF-7 CELL

The experimental measurements of Strobl *et al.* [8] led to formulate a model, in which potassium ion channels activity play an important role in regulating the membrane potential of the breast cancer cell line MCF-7 [8]. In the biological model of Strobl *et al.*, the G1/S transition is accompanied by the opening of the potassium ion channels in the membrane which leads to the flow of potassium ions outside of the cell and thus the hyperpolarization of the membrane. Changes in the potassium ion channels activity in the membrane of cancerous cells were used to explain the elevated potential on the breast skin surface above the tumor as reported in [3]. In addition, in other cancerous cells there is also a change in the rate of active transport of ions during the G1/S transition [9]. This work proposes to mathematically model the time variations in the active transport and potassium permeability, reported in the previous biological models, during the hyperpolarization phase.

III. FORMULATIONS

Cellular activities disturb the ionic charges and potential distributions which lead to the creation of diffusion and drift forces trying to return the system back to equilibrium. The three governing equations are:

$$\vec{J}_m = -D_m \nabla C_m - \mu_m C_m Z_m \nabla \varphi \tag{1}$$

$$\frac{\partial C_m}{\partial t} = -\nabla \cdot \vec{J}_m \tag{2}$$

$$\nabla^2 \varphi = -\frac{F}{\varepsilon} \sum_m Z_m C_m \tag{3}$$

where $\vec{J}_m$ is the electric current density of ion m (moles/(cm^2×s)), D_m is the diffusion coefficient of ion m (cm^2/s), C_m is the concentration of ion m (moles/cm^3), μ_m is the mobility of ion m (cm^2/(volt × s)), Z_m is the signed charge of ion m, φ is the electrostatic potential (V), F is Faraday's constant (96485 C/mol) and ε is the permittivity of the material ($\approx 80\varepsilon_0$ F/m for water). Three ions are considered: Potassium, C_{K^+}, Sodium, C_{Na^+}, and Chloride, C_{Cl^-}, due to the important role they play in regulating the

membrane potential. A fourth ion named C_{A^-} is added in only the pixels corresponding to cancerous cells to account for the intracellular negatively charged proteins. The value of C_{A^-} is set equal to 135mM comparable to the value in human cells [10]. Unlike the three other ions, negatively charged proteins cannot penetrate the cell membrane and therefore the value of C_{A^-} is fixed during the simulation.

Equations (1)-(3) are discretized using the $L \times L$ configuration in Fig. 1, where L is set equal to 11 and each step is equal to 10 μm, the average size of a human cell [10]. A small L is chosen to reduce the computational time without affecting the electric signals. The computational grid can be easily expanded by using a larger L, at the expense of larger computational time. A single cell MCF-7 cell is modeled at the center of the grid; however it is not limited to be at the center.

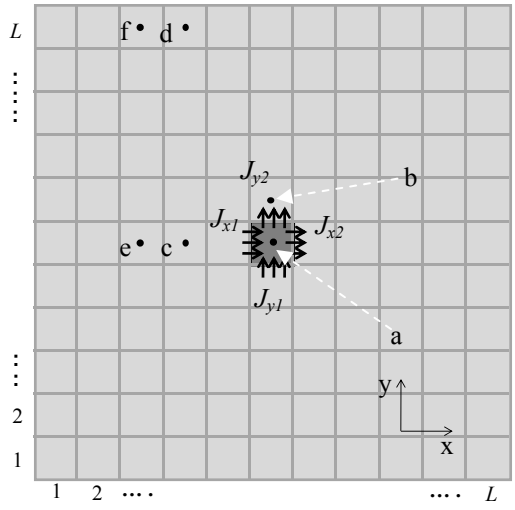

Fig. 1. The model configuration showing the blood vessel location (on the right), a cancerous cell (dark gray), plasma (light gray) and the tissue boundary (on the left). The arrows define the positive direction of the electric current densities used in the model.

The boundary conditions imposed on the configuration in Fig. 1 are a constant concentration of ions and constant zero potential on the right hand side. This is to emulate the presence of a blood vessel on the right hand side as in [4]. The left hand side of the model represents a tissue boundary where all fluxes are set equal to zero. This is to emulate the breast surface. The top and bottom boundaries are set as periodic boundary conditions following [4]. The BP difference $V_1 = \varphi_a - \varphi_b$ represents the difference between the inside and outside of the cell. The BP differences $V_2 = \varphi_c - \varphi_d$ and $V_3 = \varphi_e - \varphi_f$ are defined as the BP difference between a point adjacent to the tumor cell and a point distant from it similar to what is employed in the BP characterization of breast cancer [2]. φ_a, φ_b, φ_c, φ_d, φ_e, and φ_f are the BPs at the pixels a, b, c, d, e and f shown above, respectively. J_{x1}, J_{x2}, J_{y1} and J_{y2} represent the total (active +passive) electric current densities at the boundary of the cell as shown in Fig. 1. The next section, describes the solution of (1)-(3) using the configuration in Fig. 1.

A. Implicit Discretization

The implicit discretization, developed for modeling the MEtal Semiconductor Field Effect Transistor (MESFET) in [7], is adopted here due to its stability. In the implicit discretization, the potential values, φ, at each pixel are solved for the next time step *(t+1)* before evaluating the ions concentrations, C_m^{t+1}, values, and (3) is discretized as [7]:

$$\nabla^2 \varphi^{t+1} = -\frac{F}{\varepsilon} \sum_m Z_m C_m^{t+1} \tag{4}$$

The values of the ions concentration at the next time step are not known since the potential values are updated before the ion concentration values. The values of C_m^{t+1} are estimated by expanding them in terms of C_m^t values using Taylor series. By retaining the first two terms only in the Taylor series and substituting for the value of $\frac{\partial C_m^t}{\partial t}$ from the continuity equation in (2), C_m^{t+1} can be expressed as:

$$C_m^{t+1} = C_m^t - \Delta t \cdot \left(\nabla \cdot \vec{J}_m^{t,t+1} \right) \tag{5}$$

The term $\nabla \cdot \vec{J}_m^{t,t+1}$ includes φ^{t+1} and C_m^t. Substituting (5) in (4) it can be written as:

$$\nabla^2 \varphi^{t+1} = -\frac{F}{\varepsilon} \sum_m Z_m \left(C_m^t - \Delta t \cdot \nabla \cdot \vec{J}_m^{t,t+1} \right) \tag{6}$$

It is important to note that the concentration of ions and the potential share the same discretization grid. The electric current density from one pixel to an adjacent one are calculated half way at the boundary between two pixels. The diffusion and mobility coefficients are also evaluated halfway between any two pixels. One of the advantages of the above model is that it assigns different mobility and diffusivity coefficients at different regions of the grid. For example, the cell membrane of a living cell is semi-permeable and therefore will not allow ions to flow as freely as in plasma [10]. If a living cell is located at pixel (*I, J*) the diffusivity (Db_m) and the mobility (μb_m) coefficients at the cell boundaries, *(I, J+0.5)*, *(I, J-0.5)*, *(I+0.5, J)*, and *(I-0.5, J)*, are set to values much smaller than their surroundings. Equation (6) is then discretized using standard finite difference and solved at each time step. The ion concentrations are then updated using (2) and φ^{t+1}.

B. Cancerous Cell Active Transport

A pixel bearing a living cell exchanges ions with its surroundings using active transport [10]. Active transport is performed by the cell membrane and occurs in directions opposite to those of diffusion and drift forces. Equations (1-3) account for diffusion and drift forces but not for the active transport. The sodium-potassium active pump, known as the (Na^+-K^+) ATPase pump, pumps potassium into the cell and sodium out of the cell, consuming energy or ATP during the process. The (Na^+-K^+) ATPase pump is integrated

in the model due to its presence in the membranes of almost all animal cells [10]. For a cell at pixel *(i, j)*, the active influx is modeled as:

$$C_m(i,j) = C_m(i,j) + f_m \Delta_t \tag{7a}$$

$$C_m(I,J) = C_m(I,J) - f_m \Delta_t / 4 \tag{7b}$$

where *(I, J)* represent the four immediate neighbors of the cell. The pumping rate f_m for sodium ions, $\left(f_{Na^+}\right)$ and potassium ions $\left(f_{K^+}\right)$ can be modeled as [11]:

$$f_{Na^+} = -f_{\max} \times \left(\frac{C^t_{Na^+-i}}{(C^t_{Na^+-i} + K_{Na^+-i}(1 + C^t_{K^+-i} / K_{K^+-i}))} \right)^3 \times \left(\frac{C^t_{K^+-o}}{(C^t_{K^+-o} + K_{K^+-o}(1 + C^t_{Na^+-o} / K_{Na^+-o}))} \right)^2 \tag{8a}$$

$$f_{K^+} = -0.667 f_{Na^+} \tag{8b}$$

where f_{max} is the maximum pumping rate, $C^t_{Na^+-i}$ and $C^t_{K^+-i}$ refer to the intracellular sodium and potassium concentrations, respectively and $C^t_{Na^+-o}$ and $C^t_{K^+-o}$ refer to the extracellular sodium and potassium concentrations, respectively. The K_{Na^+-i}, K_{K^+-i}, K_{K^+-o} and K_{Na^+-o} factors are termed *dissociation coefficients*. The exact values for these coefficients for the MCF-7 cells are, to the best of our knowledge unknown. As an estimate, their values are set equal to those of red blood cells reported in [11]. The next section outlines the values of the parameters used in (1)-(8) above.

C. f_{max}, Db_m and μb_m for simulating the reference, depolarization and hyperpolarization state

This model focuses on calculating the electric signals induced by the MCF-7 cell due to the hyperpolarization in the G1/S transition. Before the hyperpolarization state is simulated, the model passes first through the reference state, which represents the cell status before division, followed by the depolarization state which occurs early in the G1 state.

In all the three states, the concentrations C_{K^+}, C_{Na^+}, and C_{Cl^-} in the blood pixels are fixed equal to 5, 155 and 160*mM*, respectively which is comparable to those reported in [10]. At all pixels, other than the cell boundary, the diffusion coefficients D_{k^+}, D_{Na^+} and D_{Cl^-} are set equal to 1.96×10^{-5}, 1.33×10^{-5} and 2.03×10^{-5} cm^2s^{-1}, respectively and the mobility coefficients μ_{k^+}, μ_{Na^+} and μ_{Cl^-} are set equal to 7.62×10^{-4}, 5.19×10^{-4} and 7.92×10^{-4} $cm^2/(sV)$, respectively. Since plasma is mostly composed by water, the diffusivity and mobility coefficients are selected equal to the values in water as in [12]. Uniform distribution of ions concentrations at values equal to those in blood and zero potential at all pixels is used for the initial conditions.

The three main parameters which control the cell state are f_{max}, Db_m and μb_m. In the reference state, f_{max} =2mMs^{-1}, $Db_{k^+} = 7.84\times10^{-9}$, $Db_{Na^+} = 0.665\times10^{-9}$, $Db_{Cl^-} = 3.25\times10^{-9}$ cm^2s^{-1}, $\mu b_{k^+} = 3\times10^{-9}$, $\mu b_{Na^+} = 0.257\times10^{-9}$, μb_{Cl^-} =1.255×10^{-7} $cm^2s^{-1}V^{-1}$. The values of the previous factors are chosen to produce realistic intracellular ionic concentrations and membrane potential at the three stages and they are comparable with those in other cancer cells [9].

In the depolarization state, f_{max} is reduced by four times whilst Db_{k^+} and μb_{k^+} are reduced by ten times. The other parameters are maintained constant. In the hyperpolarization state f_{max}, Db_{k^+} and μb_{k^+} are returned back to their reference state values. The change in the maximum transport rate f_{max} is comparable to what happens in other cancerous cells such as neuroblastoma [9]. The changes in Db_{k^+} and μb_{k^+} are consistent with the ten-time change in potassium permeability in MCF-7 cells reported in [13].

Based on experimental measurements, the time profile of the membrane potential of MCF-7 cells during the hyperpolarization state was defined in [8] but not its duration. Therefore, two time durations, 0.6 hours and 6 hours, for the hyperpolarization state are modeled. The change in the f_{max}, Db_{k^+} and μb_{k^+} is simulated to have a slow rate of change at the beginning, a sharp transition in the middle, and a slow rate of change at the end such that the simulated membrane potential (V_1) profile in both durations matched the membrane potential profile of MCF-7 cells [8].

IV. NUMERICAL RESULTS

Fig. 2a and 2b shows the BP difference V_1 defined in Fig. 1 compared to the BP difference in [8] for the 0.6 hours and 6 hours durations, respectively. The generated profiles show good agreement with [8] in terms of both the shape and the values of the membrane potential at the start and end of the hyperpolarization phase. This validation gives confidence to the values of the parameters selected.

The BPs differences V_2 and V_3 and the electric current densities J_{y1} and J_{y2} are plotted for the two time durations in Fig. 3 and Fig. 4, respectively. It is clear that the faster the hyperpolarization state, the higher the BP differences V_2 and V_3 and the higher the electric current density J_{y1} and J_{y2}. This is true of the other electric signals defined in Fig. 1. Therefore, malignant tumors, which tend to divide faster, will produce higher electric signals than benign tumors. Also, V_3 is less than V_2 which is expected since it is further from the tumor. Due to space limit, the other electric signals defined in Fig. 1 will be presented in the conference. The calculation of the previously described electric signals at the

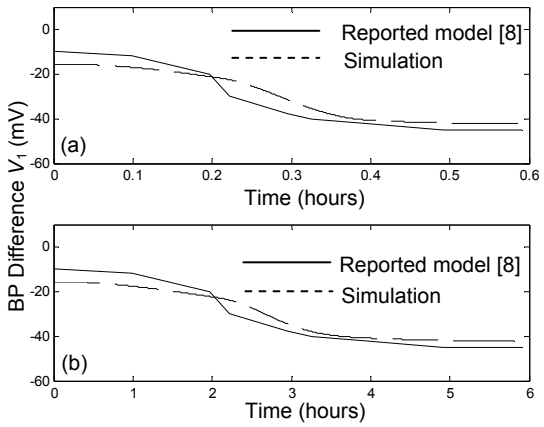

Fig. 2. The profile of the simulated and reported BP difference (V_1) during the hyperpolarization phase for two time durations a) 0.6 hours and b) 6 hours.

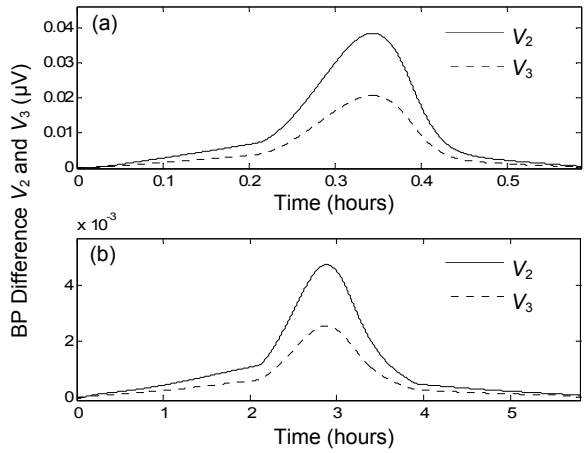

Fig. 3. Variation in V_2 (solid) and V_3 (dotted) during the hyperpolarization state for a) 0.6 hours and b) 6 hours hyperpolarization duration.

boundary or in the surroundings of the MCF-7 cell represents the main contribution of this work.

V. Conclusion and Future Work

A diffusion drift model is developed to simulate the electric signals generated by a MCF-7 cell. The model shows that the faster the transition, the higher the generated electric signals.

Ongoing research is currently performed to extend the model into a multi-cellular cancer seed. Significant evidence exists in the literature to support the fact that intercellular communication is significantly reduced between cancerous cells in a primary tumor in comparison to healthy cells [14]. This reduced intercellular communication is due to the loss in the expression of connexins (such as Cx26 and Cx43) in cancerous cells constituting the primary tumor [14]. Connexins constitute the gap junctions responsible for intercellular communication in healthy cells. Hence, as a first approximation more cells will be introduced to the configuration in Fig. 1 and each cell will not exchange ions with its neighboring cancerous cells. The intercellular

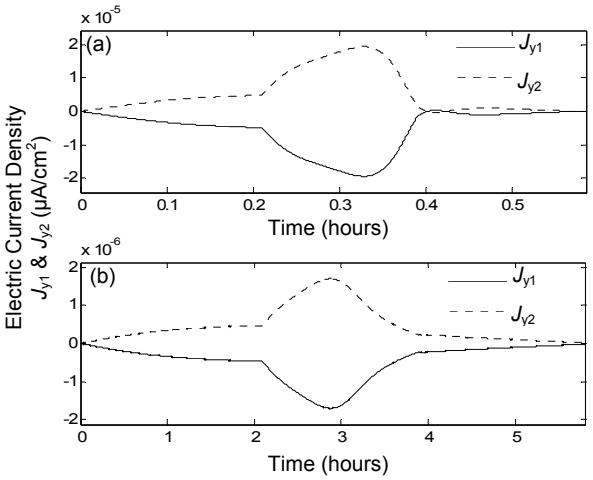

Fig. 4. Variation in J_{y1} (solid) and J_{y2} (dotted) during the hyperpolarization state for a) 0.6 hours and b) 6 hours hyperpolarization duration.

exchange of ions between adjacent cancerous cells will be then set to various coefficients (much lower than those between the cancerous cell and plasma) to study its effect on tumor patterns and the generated electric signals.

References

[1] A. Kotini, A. Anastasiadis, N. Koutlaki, D. Tamiolakis, P. Anninos, P. Anastiadis, "Biomagnetism in gynaecologic oncology. Our experience in Greece," *Eur. J. Gyn. Oncol.*, vol. 27, no. 6, pp. 594-596, 2006.

[2] J. Cuzick *et. al.*, "Electropotential measurements as a new diagnostic modality for breast cancer," *The Lancet*, vol. 352, Aug., 1998.

[3] A. Marino, D. Morris, M. Schwalke, I. Iliev and S. Rogers, "Electrical Potential Measurements in Human Breast Cancer and Benign Lesions," *Tumor Biology*, vol. 15, pp. 147-152, 1994.

[4] S. Ferreira Junior, M. Martins and M. Vilela, "Reaction-diffusion model for the growth of avascular tumor," *Physical Review E*, vol. 65, no. 2, pp. 021907-1 021907-8, 2002.

[5] John Clark and R. Plonsey, "A mathematical evaluation of the core conductor model," *Bioph Journal*, vol. 6, pp. 95-112, Jan. 1966.

[6] A. M. Hassan and M. El-Shenawee, "Diffusion-Drift Modeling of a Growing Breast Cancerous Cell," *accepted for publication in the IEEE Trans. on Biomed. Eng.*

[7] S. Yoganathan and S. Banerjee, "A New Decoupled Algorithm for Nonstaionary, Transient Simulations of GaAs MESFET's," *IEEE Trans. on Elect. Dev.*, vol. 39, pp. 1578-87, July 1992.

[8] J. Strobl, W. Wonderlin and D. Flynn, "Mitogenic Signal Transduction in Human Breast Cancer Cells," *Gen. Pharmac.*, vol. 26, no. 8, pp. 1643-1649, 1995.

[9] J. Boonstra, C. Mummery, L. Tertoolen, P. Van Der Saag and S. Laat, "Cation transport and growth regulation in neuroblastoma cells. Modulations of K+ transport and electrical membrane properties during the cell cycle," *J. Cell. Phys.*., vol. 107, no. 1, pp. 75-83, 1981.

[10] H. Lodish *et. al.*, *Molecular Cell Biology*, Fifth edition, W. H. Freeman, pp. 19, 2003.

[11] V. Lew and R. Bookchin, "Volume, pH, and Ion-Content Regulation in Human Red Cells: Analysis of Transient Behavior with an Integrated Model," *J. Memb. Biol.*, vol. 92, pp. 57-74, 1986.

[12] B. Hille, *Ion Channels of Excitable Membranes*, Third Edition, Sinauer Associates, Inc., 2001.

[13] W. Wonderlin, K. Woodfork, and J. Strobl, "Changes in Membrane Potential During the Progression of MCF-7 Human Mammary Tumor Cells Through the Cell Cycle," *J. Of Cell. Phys.*, vol. 165, pp. 177-185, 1995.

[14] E. McLachlan, Q. Shao and D. Laird, "Connexins and Gap Junctions in Mammary Gland Development and Breast Cancer Progression," *J Mem. Biol*, vol. 218, pp. 107-121, 2007.